ETH zürich

ETH Library

Evaluation of Downward Surface Longwave Flux Estimates Using Meteosat Cloud Observations

Journal Article

Author(s):
Lopes, Francisco M.; Dutra, Emanuel; Trigo, Isabel F.; Wild, Martin

Publication date:
2024-03-28

Permanent link:
https://doi.org/10.3929/ethz-b-000667309

Rights / license:
Creative Commons Attribution-NonCommercial 4.0 International

Originally published in:
Journal of Geophysical Research: Atmospheres 129(6), https://doi.org/10.1029/2023JD040306

This page was generated automatically upon download from the ETH Zurich Research Collection.
For more information, please consult the Terms of use.

Check for updates

JGR Atmospheres

RESEARCH ARTICLE
10.1029/2023JD040306

Evaluation of Downward Surface Longwave Flux Estimates Using Meteosat Cloud Observations

Francisco M. Lopes[1,2], **Emanuel Dutra**[1,2], **Isabel F. Trigo**[1,2], **and Martin Wild**[3]

[1]Instituto Português do Mar e da Atmosfera, IPMA, Lisbon, Portugal, [2]Instituto Dom Luiz, IDL, Faculty of Sciences, University of Lisbon, Lisbon, Portugal, [3]ETH Zürich, Institute for Atmospheric and Climate Science, Zürich, Switzerland

Key Points:

- Evaluation of a new high spatial (0.05°) and temporal (30 min) resolution DSLF product constrained by MSG satellite cloud information
- The new DSLF MARS product outperforms the current LSA SAF when evaluated against 48 ground stations
- High level of spatial and temporal variability consistency between four DSLF products MARS, LSA SAF, ERA5, CERES

Supporting Information:

Supporting Information may be found in the online version of this article.

Correspondence to:

F. M. Lopes,
francisco.lopes@ipma.pt

Citation:

Lopes, F. M., Dutra, E., Trigo, I. F., & Wild, M. (2024). Evaluation of downward surface longwave flux estimates using Meteosat cloud observations. *Journal of Geophysical Research: Atmospheres*, *129*, e2023JD040306. https://doi.org/10.1029/2023JD040306

Received 3 NOV 2023
Accepted 6 MAR 2024

Author Contributions:

Conceptualization: Emanuel Dutra, Isabel F. Trigo
Data curation: Francisco M. Lopes, Emanuel Dutra
Formal analysis: Francisco M. Lopes, Martin Wild
Funding acquisition: Emanuel Dutra, Isabel F. Trigo
Investigation: Francisco M. Lopes, Emanuel Dutra, Isabel F. Trigo, Martin Wild
Methodology: Francisco M. Lopes, Emanuel Dutra, Isabel F. Trigo
Project administration: Emanuel Dutra, Isabel F. Trigo

© 2024 The Authors.
This is an open access article under the terms of the Creative Commons Attribution-NonCommercial License, which permits use, distribution and reproduction in any medium, provided the original work is properly cited and is not used for commercial purposes.

Abstract The downward surface longwave flux (DSLF) plays a relevant role in the Earth's surface radiative budget, which is crucial to monitor, understand and model the impact of changes at local and global scales on surface temperature and surface conditions. This study focuses on the evaluation and intercomparison of four DSLF products: (a) a recently developed all-weather DSLF product based on the multivariate adaptive regression splines (MARS) algorithm driven by satellite cloud information from the Meteosat Second Generation (MSG) and ERA5 reanalysis screen variables; (b) the Satellite Application Facility on Land Surface Analysis (LSA SAF); (c) CERES Synoptic top-of-atmosphere and surface fluxes and clouds (CERES-SYN1deg) and (d) ERA5 reanalysis. The study covers the period 2005–2021 and the MSG region focusing on monthly means. The evaluation performed against 48 ground stations from the Baseline Surface Radiation Network (BSRN) and FLUXNET2015 networks showed that the MARS product outperforms the remaining products, particularly the LSA SAF, while ERA5 and CERES show similar performance metrics. The fours products are intercompared in terms of their mean spatial variability and temporal mean annual cycles and inter-annual variability in four selected regions, showing a high level of agreement, particularly between MARS, ERA5 and CERES. Our results highlight the clear added value of MARS with respect to LSA SAF, while providing higher spatial resolution (0.05°), constrained by satellite cloud information, when compared with ERA5 (0.25°) or CERES (1°).

Plain Language Summary Radiation that reaches the Earth's surface is fundamental for our understanding of the Earth's energy balance. In this work, we use a complex mathematical method together with data from weather satellites and ground-based instruments to estimate the heat radiation component. To evaluate our results, we perform a comparison with those from various existing methods, including the one used by the Portuguese meteorological service. Our method generally outperforms the already existing techniques, with small errors as compared to surface measurements, demonstrating the added value of this new approach in improving our understanding of Earth's energy budget.

1. Introduction

The energy balance at the Earth's surface, that is, the balance between net radiation and heat fluxes at any given time and place, is key in determining the spatial distribution and temporal evolution of surface temperature (Liou, 2002). Observations or observation-based estimates of the different components of the surface radiation budget are therefore important to monitor, understand and model the impact of changes at local and global scales on surface temperature and surface conditions, in general (e.g., Feng, Zhang, et al., 2020, 2023; Houghton et al., 2001; Wang & Dickinson, 2013). In particular, downward surface longwave fluxes (hereafter DSLF), that is, the thermal radiation (4–100 μm) emitted by the atmosphere that reaches the surface, play a relevant role in the Earth's surface radiative budget (Wild et al., 2013), allowing to control the night-time radiative cooling (e.g., Hoch et al., 2011), which can reach values that are comparable to solar radiation in daytime under cloudy conditions (e.g., Ojo et al., 2019).

In order to continuously measure DSLF, ground stations equipped with state-of-the-art instrumentation such as pyrgeometers (Meloni et al., 2012) are used. Most of the available stations are scattered across the globe (typically unevenly distributed), being often installed in regions of higher population density, generally in mid-latitudes of the northern hemisphere (NH), leading to an uneven geographical distribution of observational datasets based on in situ measurements. These can also be limited, mostly due to equipment and maintenance costs, with only a small number of stations being actually dedicated to surface radiation observations, for instance the usually

21698996, 2024, 6, Downloaded from https://agupubs.onlinelibrary.wiley.com/doi/10.1029/2023JD040306 by ETH Zurich, Wiley Online Library on [08/04/2024]. See the Terms and Conditions (https://onlinelibrary.wiley.com/terms-and-conditions) on Wiley Online Library for rules of use; OA articles are governed by the applicable Creative Commons License

Resources: Emanuel Dutra, Isabel F. Trigo
Supervision: Emanuel Dutra, Isabel F. Trigo
Validation: Francisco M. Lopes
Visualization: Francisco M. Lopes, Emanuel Dutra, Isabel F. Trigo
Writing – original draft: Francisco M. Lopes
Writing – review & editing: Francisco M. Lopes, Emanuel Dutra, Isabel F. Trigo, Martin Wild

referenced Baseline Surface Radiation Network (BSRN, Driemel et al., 2018). Moreover, some of these stations can be located in remote areas of difficult access that do not provide the required conditions for their regular maintenance, thus not allowing to perform a correct assessment of DSLF. Since DSLF is primarily determined by emission in the lowest portion of the atmospheric boundary layer, that is, within the first hundred meters above the Earth's surface (Zhao et al., 1994), satellite observations are only indirectly related with DSLF. However, it has been previously shown that estimates based solely on satellite observations can be computed, allowing to perform studies not only at remote locations but also over larger areas (e.g., Cheng et al., 2017; Jiao, 2022). Despite this advantage compared to in situ, satellite estimates of DSLF are difficult and typically associated with significant uncertainties, relying on the satellite interpretation of clouds and associated errors (Ellingson, 1995). In addition to a very high dependency on the vertical profiles of atmospheric air temperature and, most noticeably, water vapor, DSLF variability is significantly influenced by cloud-base properties (height, temperature, and emissivity), by increasing the total effective emissivity of the sky. Therefore, a correct estimation of DSLF requires an accurate characterization of these parameters, which cannot be adequately addressed only with satellite observations.

Numerical weather prediction (NWP) models, such as those used in reanalyzes, provide spatially complete DSLF estimates at sub-daily temporal frequencies covering long periods of time (Wild et al., 2001). However, these are usually hampered by uncertainties due to high sensibility toward the longwave flux parameterization used on the one hand, and to the sensitivity to model variables which are also often prone to significant errors, such as cloud cover and type. To reduce uncertainty under such conditions, NWP variables can be blended with remotely sensed information, which is often more reliable in characterizing cloud patterns and their temporal evolution, through the use of empirical or semi-empirical methods (e.g., Diak et al., 2000; Iziomon et al., 2003; Trigo et al., 2010; Wang & Dickinson, 2013; Zeng et al., 2020; Zhong et al., 2019), relying on large datasets to derive those relationships and algorithms to estimate DSLF. In recent decades, there has been an increasing use of this approach to derive DSLF, namely based on multiple regression models (e.g., Trigo et al., 2010; Zeng et al., 2020) and, more recently, machine learning models (e.g., Cao et al., 2022; Feng, Ye, & Zou, 2020; Feng, Zhang, et al., 2020; Feng et al., 2021; Jiang et al., 2022; Lopes et al., 2022; Shao et al., 2023; Wang et al., 2012, 2020; Zhou et al., 2018, 2019; Jung et al., 2019), which are able to account for complex nonlinear interactions that occur between DSLF and respective predictors. The latter can be separated into different branches, including artificial neural network (e.g., Feng, Ye, & Zou, 2020; Feng, Zhang, et al., 2020; Jiang et al., 2022; Wang et al., 2012), random forest (e.g., Shao et al., 2023; Wang et al., 2020), extremely randomized trees (e.g., Cao et al., 2022), gradient boosting regression tree (e.g., Feng et al., 2021), and multivariate adaptive regression splines (MARS, e.g., Jung et al., 2019; Lopes et al., 2022; Zhou et al., 2018, 2019). For instance, Jiang et al. (2022) used a generic algorithm-artificial neural network to create a model that combines DSLF data simulated by the Moderate Resolution Atmospheric Transmittance and Radiance Code (MODTRAN-5) with satellite information (radiance at top-of-atmosphere, cloud mask, and water vapor content) from the Moderate-resolution Imaging Spectroradiometer (MODIS) and ERA5 reanalysis (cloud base height and temperature, total cloud cover, 2-m air and dew point temperatures) to produce estimates of DSLF under cloudy-sky conditions. When evaluated against different observational network sites, the accuracy of the estimated DSLF was shown to have a strong dependency on the estimation of cloud base height and near-surface air temperature. Indeed, the uncertainty generated from cloud base height retrieval through remote sensing was highlighted by Shao et al. (2023) when estimating hourly DSLF values using a random forest algorithm under cloudy conditions, from which a better performance was attained in comparison to ERA5 and CERES. Daily datasets of DSLF with a 5-km spatial resolution based on a combination of a gradient boosting regression tree algorithm with DSLF observations from 4 different networks, ERA5 variables (2-m air temperature, relative humidity at 1,000 hPa, and total column water vapor), and satellite surface downward shortwave radiation, were evaluated by Feng et al. (2021). The corresponding results showed higher daily errors than monthly DSLF aggregations, as expected. With the latter, the authors showed that the performance of the proposed model surpasses that of other existing models or satellite-based products, including ERA5 and CERES Synoptic top-of-atmosphere and surface fluxes and clouds (CERES-SYN). To validate the accuracy of different machine learning methods in estimating DSLF, Feng, Ye, and Zou (2020) and Feng, Zhang, et al. (2020) combined MARS with BSRN observations to train their model to produce daily and monthly DSLF values. The differences found between the MARS model and the remaining models were small, highlighting the need for a better optimization of model parameters and input variables selection, although it should be stressed that the considered models did not use remotely sensed information. Zhou et al. (2018, 2019) made use of a MARS algorithm combined with MODIS thermal infrared bands top-of-atmosphere radiances and observations

21698996, 2024, 6, Downloaded from https://agupubs.onlinelibrary.wiley.com/doi/10.1029/2023JD040306 by ETH Zurich, Wiley Online Library on [08/04/2024]. See the Terms and Conditions (https://onlinelibrary.wiley.com/terms-and-conditions) on Wiley Online Library for rules of use; OA articles are governed by the applicable Creative Commons License

from 6 different networks to produce estimates under clear-sky conditions only. The validation results yield a comparable accuracy of the MARS model to other existing products, being attained using an independent group of observational sites. More recent efforts toward the use of a high spatial resolution algorithm that enables the combination of cloud information from remotely sensed data with ground observations and reanalysis data have been achieved by Lopes et al. (2022), being the starting point of the present study.

In this work, we propose the combination of remotely sensed observations and near surface (2-m air and dew point temperatures) and bulk (total column water vapor) variables derived from state-of-the reanalysis to compute DSLF for all-sky conditions. In particular, we aim to produce instantaneous values (at 30-min frequency) of DSLF for the whole disc observed by the Meteosat Second Generation (MSG) satellite series, within the framework of the European Organization for the Exploitation of Meteorological Satellites (EUMETSAT) Satellite Application Facility on Land Surface Analysis (LSA SAF) operations. For that purpose, we use the MARS algorithm, previously calibrated with in situ observations, to estimate DSLF, which, as described by Lopes et al. (2022), provided a good performance with very satisfactory results. The MARS algorithm was trained with BSRN observations of DSLF from 23 ground stations, air and dewpoint temperatures and water vapor gathered from the European Centre for Medium-range Weather Forecasts (ECMWF) latest reanalysis (ERA5), while cloud information was obtained from the MSG satellite to compute separately DSLF for clear and cloudy-sky conditions. Besides providing a good performance when evaluated against ground observations, the MARS algorithm was also shown to outperform other DSLF products, including the current LSA SAF operational algorithm. Moreover, an additional evaluation against an independent network of 52 ground observations from FLUXNET2015 (Pastorello et al., 2020), highlighted the improvements attained in estimating hourly DSLF values with MARS in comparison to other existing products, demonstrating the algorithm accuracy in its application over different locations than the ones used during the training stage. Although MARS DSLF estimates typically yield lower errors, they also exhibit characteristic errors, similarly to the other DSLF products (Silber et al., 2019). In particular, the algorithm was shown to produce an overall overestimation of hourly DSLF estimates for clear-sky conditions, and an underestimation for cloudy conditions. Despite this behavior, a general improvement is found when directly compared with LSA SAF operational product.

This study focuses the evaluation and intercomparison of four DSLF products: (a) the recently developed all-weather DSLF product based on the MARS algorithm driven by satellite cloud information from the MSG and ERA5 reanalysis screen variables; (b) the LSA SAF; (c) CERES-SYN1deg and (d) ERA5. The study covers the period 2005–2021 and the MSG region focusing on monthly means. The first part of the work addresses the evaluation, which is performed against 48 ground stations from the BSRN and FLUXNET2015 networks. The second part focuses on the four products' intercomparison in terms of their mean spatial variability and temporal mean annual cycles and inter-annual variability in four selected regions. It should be noted that this procedure is an important step within the framework of LSA SAF operations, with the aim of supporting the transition from the current (and outdated) operational algorithm to a new algorithm as LSA SAF product for DSLF. Taking advantage of the MARS flexibility, such implementation will also benefit from the use of satellite information acquired through the Meteosat Third Generation satellite for operational purposes, which will enable higher temporally and spatially resolved DSLF products.

The remaining structure of this paper is given as follows: data curation and the adopted methodology are presented in Section 2; the main results are shown in Section 3, with the respective discussion being provided in Section 4; final remarks are given in Section 5, while additional material related to the analysis is available in the Supporting Information S1.

2. Data and Methodology

2.1. Observational Data

Evaluation of DSLF products is performed using ground stations provided by two separate databases: BSRN (Driemel et al., 2018) and FLUXNET2015 (Pastorello et al., 2020). BSRN data (https://bsrn.awi.de/; accessed on 22 January 2024) are often used for downward longwave radiation studies (e.g., Obot et al., 2019; Roesch et al., 2011; Wild et al., 2001; Zhang et al., 2015), serving as reference for radiation measurements over the last decades, given the high-quality standards for the measured data. In the present work, following the data preprocessing (described further on), measured data from 17 (out of 57 in total) operational BSRN ground stations (temporally aggregated to hourly and then to monthly values) is used to validate DSLF estimates produced

21698996, 2024, 6, Downloaded from https://agupubs.onlinelibrary.wiley.com/doi/10.1029/2023JD040306 by ETH Zurich, Wiley Online Library on [08/04/2024]. See the Terms and Conditions (https://onlinelibrary.wiley.com/terms-and-conditions) on Wiley Online Library for rules of use; OA articles are governed by the applicable Creative Commons License

Table 1
DSLF Products Used to Compare the MARS Estimates Within the MSG Disc, Including the LSA SAF Operational Product (MDSLF), ERA5, and CERES

Product	Algorithm	Coverage	Spatial res.	Frequency	Cloud info.
MARS	Multivariate adaptive regression splines	MSG disc (lat./lon. ± 75° E/N)	0.05°	30-min	MSG (SEVIRI) cloud fraction
MDSLF	Bulk parameterization scheme + piecewise regression				
ERA5	Reanalysis	Global	0.25°	Hourly	ERA5 model cloud information
CERES	Radiative transfer model		1°	Monthly	Terra and Aqua (MODIS) cloud properties

Note. Product details are provided respectively.

with the MARS algorithm considering a 19-year period (from 2004 to 2022). The FLUXNET2015 data (https://fluxnet.org; accessed on 22 January 2024) includes 30-min measurements of DSLF (temporally aggregated to hourly and then to monthly values) from 28 ground stations comprising a 11-year period (from 2004 to 2014). All selected stations are within the MSG disc (i.e., longitude/latitude ± 75°E/N), being mostly located within the European region. More details concerning each station information are available from Lopes et al. (2022), in which both observational networks were used for an initial hourly assessment of DSLF estimates produced with the MARS algorithm.

2.2. Satellite and Model Data

To evaluate the MARS algorithm performance in estimating DSLF computed from instantaneous values for the whole MSG disc, several DSLF products are used for comparison. These include the LSA SAF current operational algorithm, as well as radiation fluxes from ERA5 and CERES. A summary of all DSLF products used in this study is provided in Table 1.

2.2.1. MARS Downwelling Longwave Radiation

The MARS core algorithm (Friedman, 1991; Friedman & Roosen, 1995) is based on a weighted sum of piecewise functions (also known as hinge functions), following a recursive partitioning form that results in a series of regression coefficients that can then be used to better adjust predictions to the data considering the maximum reduction in sum-of-squares residual error. Subsequent to the training procedure, the least effective terms are then removed within the algorithm at each step to avoid model overfitting. Here, we use the previously calibrated MARS algorithm, considering a random selection of 6 months of input data (or 40% of the available information) from each of the 23 ground stations used, corresponding to a DSLF sample range of about 5.87 years (Lopes et al., 2022). ERA5 hourly total column water vapor, 2-m air and dewpoint temperatures, together with MSG cloud fraction, were used as predictors during the calibration procedure. Cloud fraction information, retrieved from the Spinning Enhanced Visible and Infrared Imager (SEVIRI) sensor on board the MSG satellite every 15-min, is primarily used for sky classification purposes, allowing to calibrate separately the DSLF computation for clear and cloudy conditions on a pixel level. As previously mentioned, the MARS algorithm showed a good performance, with the ability to produce hourly values of DSLF with a closer approximation to observations in comparison to the estimates produced with other products, including the LSA SAF operational algorithm. The validation analyses performed with BSRN and FLUXNET2015 showed that DSLF hourly estimates produced with the MARS algorithm generally have lower errors and higher correlations than other products, particularly for conditions where higher samples of observed DSLF exist.

In this study, the potential of MARS DSLF estimates is further exploited, particularly to serve as LSA SAF operational product. To this end, MARS DSLF calculations are now performed for the whole MSG disc at the 30-min frequency over a high-resolution regular grid (0.05°), out of which hourly, daily, and monthly mean values can then be computed for evaluation. The setup configuration to produce DSLF over the MSG disc is similar to the one used for the LSA SAF operational algorithm, being directly fed with ERA5 hourly data (total column water vapor, 2-m air and dewpoint temperatures) interpolated to 30-min time steps and sky classification (clear sky, cloudy, partially cloudy), which is available with a frequency of up to 15-min information from MSG/SEVIRI. It should be noted that in this work, the applied method only considers 30-min cloud information, where MARS DSLF values are estimated using separately the previous obtained clear/cloud MARS set of regression

21698996, 2024, 6, Downloaded from https://agupubs.onlinelibrary.wiley.com/doi/10.1029/2023JD040306 by ETH Zurich, Wiley Online Library on [08/04/2024]. See the Terms and Conditions (https://onlinelibrary.wiley.com/terms-and-conditions) on Wiley Online Library for rules of use; OA articles are governed by the applicable Creative Commons License

coefficients, depending on the sky classification of each MSG/SEVIRI pixel; as well as an equal weight that is given to both MARS cloudy and MARS clear DSLF estimates in the case the pixel is classified as partially cloudy.

2.2.2. LSA SAF Downwelling Longwave Radiation

The current LSA SAF operational product for DSLF (MDSLF, Trigo et al., 2011) is based in a bulk parameterization scheme which follows a piecewise regression, using the same inputs as MARS: total column water vapor, 2-m air and dewpoint temperatures and cloud fraction. The algorithm was previously calibrated (Trigo et al., 2010) using atmospheric profiles of temperature and humidity from the Thermodynamic Initial Guess Retrieval (TIGR, Chevallier et al., 2000) based on ERA-40, and downward infrared flux simulations from the MODTRAN-4 (Berk et al., 2003). When compared with downward longwave flux observations, the MDSLF algorithm showed an overall underestimation, which is particularly pronounced for low DSLF values. This effect is closely related to the LSA SAF original calibration, especially to the synthetic radiation flux data used from MODTRAN-4. Consequently, larger deviations between the MDSLF estimates and station observations are usually observed at very high-latitude regions (Lopes et al., 2022; Trigo et al., 2010). The MDSLF product over the whole MSG disc is available as Network Common Data Form (netCDF) in a regular 0.05° grid from 2004 to real time in the LSA SAF data service archive. Between 2004 and 2015, the product was generated using the total column water vapor and the 2-m air and dewpoint temperatures from the ERA-Interim reanalysis, while from 2016 onwards the operational real time product uses as inputs the ECMWF operational forecasts that are available at the time of production, corresponding to the +12-hr to +24-hr forecasts of the 00 and 12 UTC runs.

2.2.3. ECMWF Reanalysis

Datasets from the latest ECMWF reanalysis (ERA5, Hersbach et al., 2018) are used as inputs in both MARS and MDSLF pre-calibrated algorithms to compute DSLF for the whole MSG disc. In particular, hourly information from the atmospheric profiles of water vapor, 2-m air and dewpoint temperatures has been previously extracted from the Copernicus Data Store (https://cds.climate.copernicus.eu; accessed on 22 January 2024) to feed the MARS algorithm. In this work, the same variables, now linearly interpolated to 30-min temporal frequency, are added as inputs for the computation of DSLF within the MSG disc. All variables are bilinearly interpolated to SEVIRI/MSG pixels, while 2-m air and dew point temperatures are corrected to consider differences between the ERA5 model orography and the finer pixel-scale elevation, considering a fixed lapse rate of 0.65 K/100 m and assuming a constant dew point depression. Additionally, the ERA5 *surface thermal radiation downward* parameter (in Wm^{-2}) is also considered for comparison purposes, being available on a regular latitude-longitude grid of 0.25°. For validation purposes, it should be noted that ERA5 fluxes are adjusted according to each observation elevation using the reanalysis orography information, following a correction factor of -2.8 Wm^{-2} per 100 m (Marty et al., 2002).

2.2.4. CERES Dataset

Downward longwave fluxes, represented by the Surface longwave flux down (all-sky) parameter, from the CERES-SYN1deg product (Rutan et al., 2015), are also used in this work for comparison against the MARS estimates within the MSG disc. The CERES estimates result from the combination between CERES and MODIS instruments aboard the Terra and Aqua satellites, from which cloud properties are derived from MODIS and geostationary imager measurements to produce radiation fluxes over a 1° resolution grid. CERES estimates are used in the present analysis from February 2004 to March 2022, being retrieved from the NASA's Atmospheric Science Data Center (https://ceres.larc.nasa.gov/data/; accessed on 22 January 2024). Similarly, to ERA5 longwave radiation used for the validation procedure, CERES fluxes are also adjusted according to each observation's elevation using CERE's dataset elevation above sea level parameter, acquired separately from the hourly gridded observed top-of-atmosphere and Fu-Liou radiative transfer surface fluxes and clouds product (Doelling et al., 2016).

2.3. Methods

The evaluation of the MARS algorithm for the MSG disc is carried out using standard error metrics, including the: bias (μ), standard deviation of errors (σ), RMSE, and temporal correlation coefficient (R). The assessment is

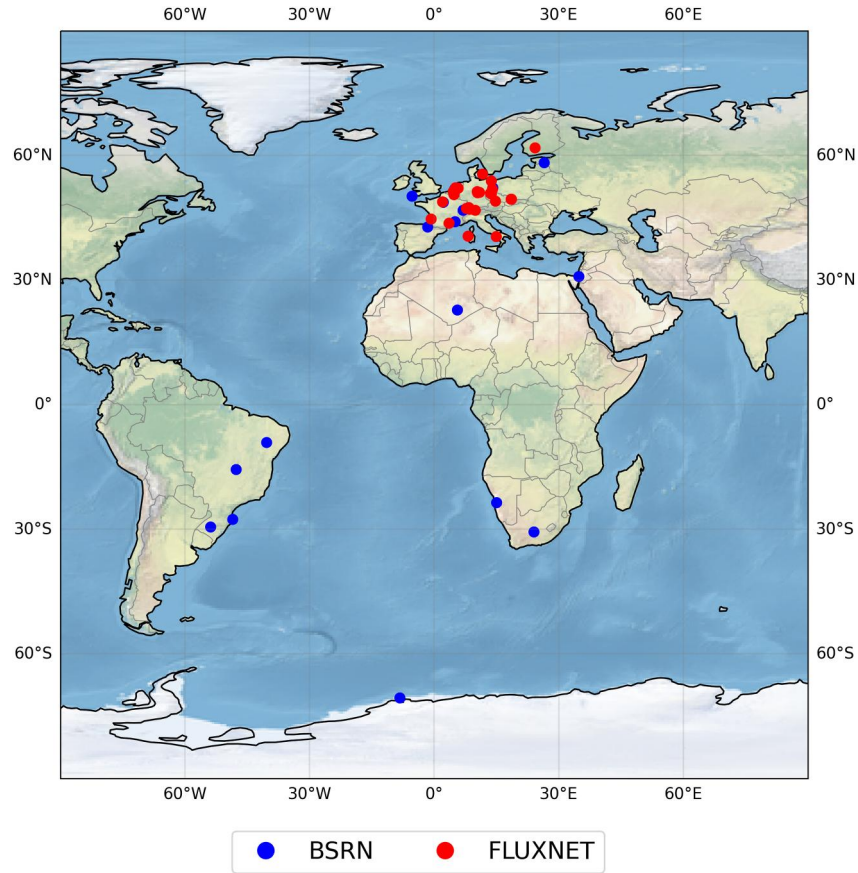

Figure 1. Location of each of the 17 Baseline Surface Radiation Network (BSRN) and 28 FLUXNET2015 ground stations within the Meteosat Second Generation satellite domain, marked by blue and red dots, respectively.

divided into two separate analyses: validation of the MARS algorithm new setup configuration for the whole MSG disc to compute DSLF against ground observations (BSRN and FLUXNET2015); and a spatio-temporal comparison of the algorithm overall performance against other products within the MSG domain.

For validation and intercomparison between products, a focus is given to monthly mean values from the beginning of the MSG data record in February 2004 to March 2022, from which a monthly validation is performed separately against BSRN and FLUXNET2015. In this context, all longwave radiation estimates are aggregated to monthly values within the available periods, that is, from 2004 to 2019 for BSRN and from 2004 to 2014 for FLUXNET2015. All gridded monthly products are then interpolated to the ERA5 regular grid (0.25°), to ease dataset intercomparison against observations, from which the nearest points to station location are selected. As described by Roesch et al. (2011), in order to avoid systematic biases, observed monthly mean values are computed for each station considering the monthly mean diurnal cycle (i.e., 24 hr) from the hourly values of each month. Moreover, for each hour value to be computed in the diurnal cycle, at least 95% of the expected hourly means must be present. To reinforce the monthly validation analyses, only stations with at least 40 months of valid data within the selected period and with a maximum elevation difference of 600 m between model/dataset grid and observation elevation are selected. As result, a total of 17 BSRN and 28 FLUXNET2015 stations were found adequate for the monthly validation analyses (Figure 1). In addition to selecting the nearest points of MARS DSLF aggregated on the 0.25° grid, the nearest point of the MARS DSLF product from the original resolution (at 0.05°) was also selected, which is denoted here as MARS*.

In the second part of the analysis, the different products are inter-compared seasonally and annually, from which regional averages are weighted by the cosine of the latitude.

21698996, 2024, 6, Downloaded from https://agupubs.onlinelibrary.wiley.com/doi/10.1029/2023JD040306 by ETH Zurich, Wiley Online Library on [08/04/2024]. See the Terms and Conditions (https://onlinelibrary.wiley.com/terms-and-conditions) on Wiley Online Library for rules of use; OA articles are governed by the applicable Creative Commons License

21698996, 2024, 6, Downloaded from https://agupubs.onlinelibrary.wiley.com/doi/10.1029/2023JD040306 by ETH Zurich, Wiley Online Library on [08/04/2024]. See the Terms and Conditions (https://onlinelibrary.wiley.com/terms-and-conditions) on Wiley Online Library for rules of use; OA articles are governed by the applicable Creative Commons License

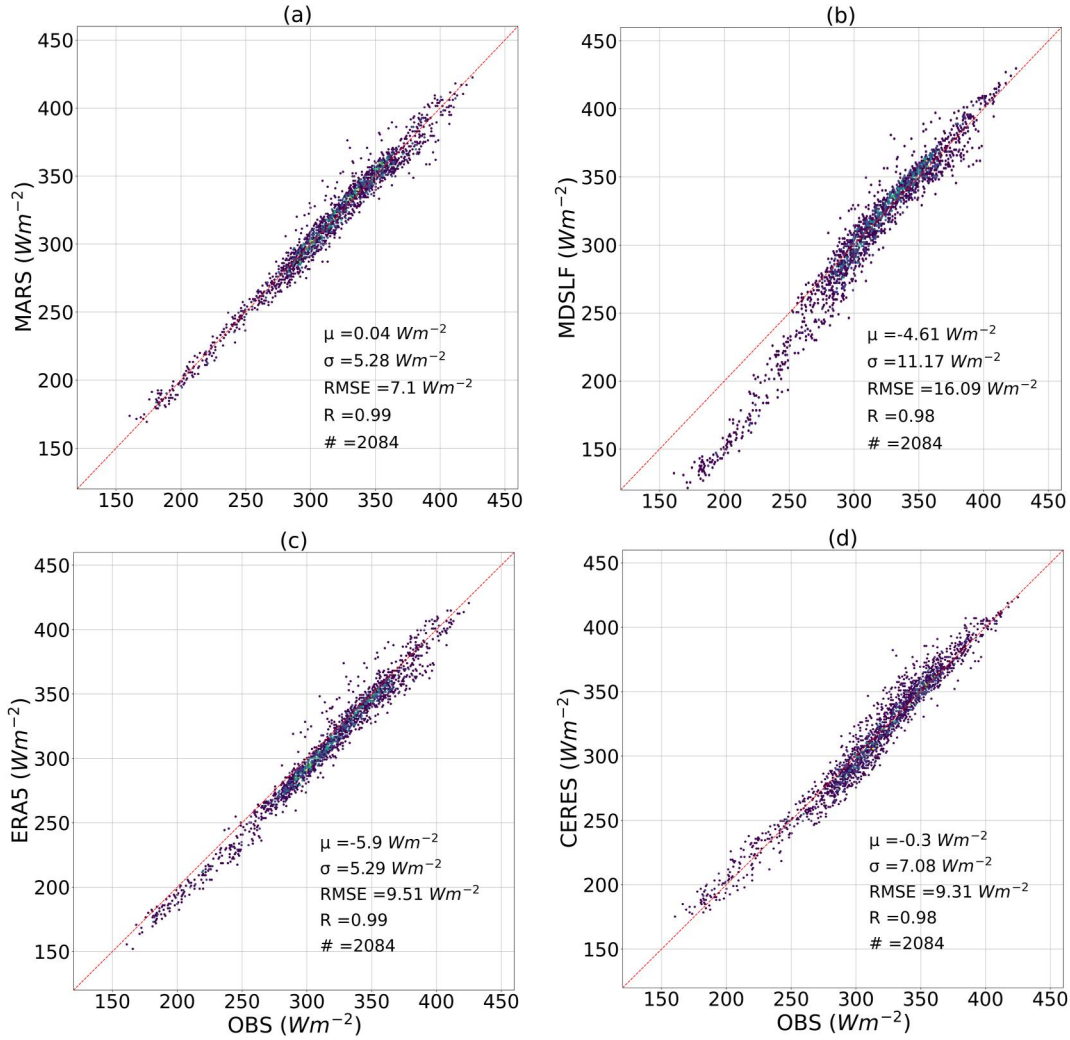

Figure 2. Scatter plots of the monthly DSLF products (vertical axis) against BSRN observations from 17 stations (horizontal axis) between 2004 and 2019: (a) MARS; (b) LSA SAF (MDSLF); (c) ERA5; and (d) CERES. All model estimates are compared against observations considering the nearest point of a 0.25° grid. Evaluation metrics are added in the lower right corner of each subplot, including the number of samples used (#), while the red dashed-lines depict the identity line. Units are in Wm^{-2}, while correlations coefficient (R) are between 0 and 1.

3. Results

3.1. Validation Against In Situ Observations

DSLF monthly estimates are evaluated separately against observations from BSRN and FLUXNET2015 ground stations within the MSG disc (Figures 2 and 3, respectively), including corresponding statistical summaries. Generally, when compared with BSRN observations from 17 ground stations (resulting in a total of 2084 monthly values), the MARS DSLF monthly estimates are shown to have relatively low errors, and are closer to the observations (Figure 2a), when compared to other DSLF products, particularly to the MDSLF (Figure 2b). The MARS DSLF bias is close to zero (0.04 Wm^{-2}) and the RMSE of 7.10 Wm^{-2} is roughly 56% lower than that of the current LSA SAF operational product. Despite relatively small errors, the MARS estimates of high longwave flux values (typically between 300 and 400 Wm^{-2}) seem to be slightly higher than observations in comparison to other products, which show an overall underestimation, particularly ERA5 and MDSLF estimates (biases of −5.90 and −4.61 Wm^{-2}, respectively). The CERES estimates present an overall low mean error (−0.30 Wm^{-2}), but higher dispersion than the MARS values. In terms of RMSE, the current LSA SAF

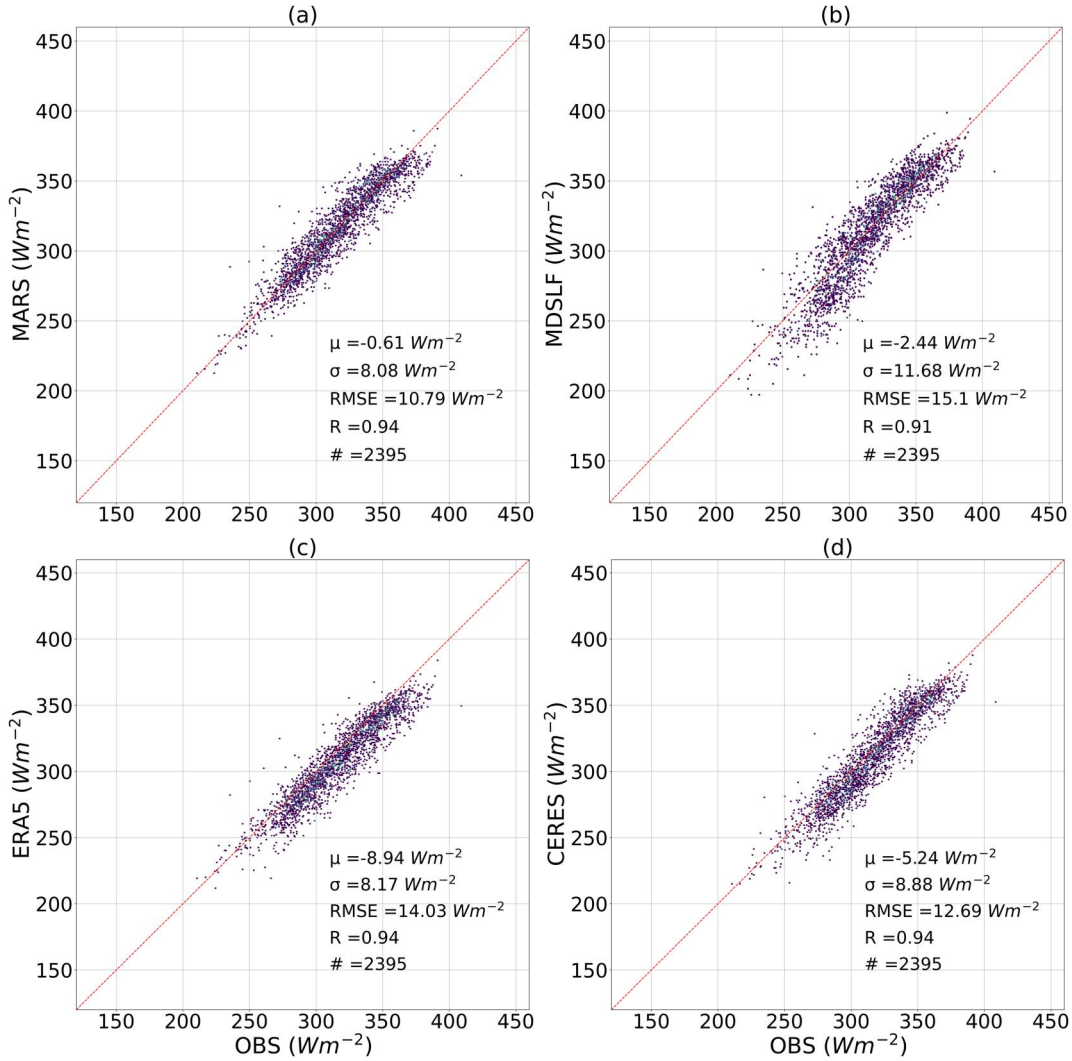

Figure 3. Similar to Figure 2 but for the FLUXNET2015 observations between 2004 and 2014.

MDSLF product presents the highest value (16.09 Wm^{-2}), while ERA5 and CERES present lower and similar values (9.51 and 9.31 Wm^{-2}, respectively). The standard deviation of errors is the lowest for MARS and ERA5 (5.28 and 5.29 Wm^{-2}, respectively), while the highest values are seen in MDSLF and CERES (11.17 and 7.08 Wm^{-2}, respectively). As clearly noticed in the corresponding MDSLF density plot (Figure 2b), there is a significant underestimation of observations for the lower range of DSLF values (i.e., between 150 and 300 Wm^{-2}), critically contributing to increase the standard deviation of errors. This is related to the LSA SAF MDSLF original algorithm calibration, particularly the synthetic radiation fluxes used from MODTRAN-4. As result, the MDSLF shows a tendency to underestimate low values of DSLF, which in this case are being depicted by one station (GVN) located at a very high latitude (about 70.65°S) in Antarctica. Regarding the MARS* performance, when the 0.05° grid nearest points to observations are directly used, the evaluation metrics (Table 2) show a small improvement in comparison with using the MARS nearest points to observations over a regular 0.25° grid. For instance, despite a small bias increase to 0.20 Wm^{-2}, there is a reduction of the standard deviation of errors and RMSE (5.16 and 6.97 Wm^{-2}, respectively), when MARS* is considered. More detailed information regarding the error metrics distributions computed independently at each BSRN station is available in Table S1 (see Supporting Information S1). It is worth noting that at the SMS station, located in Brazil, the biases are much larger in comparison to values found at other locations due to the frequent occurrence of stratiform and shallow convective clouds (Araújo Palharini & Vila, 2017), which hamper measurement and estimation of DSLF under such conditions.

21698996, 2024, 6, Downloaded from https://agupubs.onlinelibrary.wiley.com/doi/10.1029/2023JD040306 by ETH Zurich, Wiley Online Library on [06/04/2024]. See the Terms and Conditions (https://onlinelibrary.wiley.com/terms-and-conditions) on Wiley Online Library for rules of use; OA articles are governed by the applicable Creative Commons License

21698996, 2024, 6, Downloaded from https://agupubs.onlinelibrary.wiley.com/doi/10.1029/2023JD040306 by ETH Zurich, Wiley Online Library on [08/04/2024]. See the Terms and Conditions (https://onlinelibrary.wiley.com/terms-and-conditions) on Wiley Online Library for rules of use; OA articles are governed by the applicable Creative Commons License

Table 2
Statistical Summary for the Monthly Validation Between the MARS DSLF Product With Original Grid Resolution 0.05° (MARS) and Two Observational Networks (BSRN and FLUXNET2015) Considering Two Periods (2004–2019 and 2004–2014, Respectively)*

	BSRN	FLUXNET2015
μ (Wm^{-2})	0.20	−0.52
σ (Wm^{-2})	5.16	7.79
RMSE (Wm^{-2})	6.97	10.77
R (−)	0.99	0.94
#	2,084	2,395

Note. Several metrics are shown: bias (μ); standard deviation of errors (σ); root mean square error (RMSE); and correlation coefficient (R); together with the number of adequate monthly samples used (#). Units are in Wm^{-2}, while correlations are between 0 and 1.

The MARS algorithm was calibrated with a sub-set of observations from BSRN, which partially explains the good performance of the product when validated against the BSRN network. When an independent network (FLUXNET2015) of stations, providing a total of 2395 monthly values, is used the obtained results allow to assess the robustness of the MARS product (Figure 3a). As shown by the corresponding error metrics (Figure 3 and Table 2), an overall underestimation is now found in all longwave flux estimates, with the lowest bias (−0.52 Wm^{-2}) being obtained with MARS*, closely followed by MARS (−0.61 Wm^{-2}) and MDSLF (−2.44 Wm^{-2}), while CERES and, particularly ERA5, show the highest biases (−5.24 and −8.94 Wm^{-2}, respectively). The MDSLF product presents again large discrepancies with respect to observed values, especially in the lower range (for DSLF below 300 Wm^{-2}), leading to standard deviation of errors and RMSE of 11.68 and 15.10 Wm^{-2}, respectively, while the lowest standard deviation of errors is attained by MARS, particularly with MARS* (10.79 and 10.77 Wm^{-2}, respectively), being followed by ERA5 and CERES.

3.2. DSLF Products Intercomparison

The consistency of the different products is now assessed in terms of the annual mean spatial distribution over land points (Figure 4) (and seasonally, see Figures S1–S4 in Supporting Information S1). The spatial distribution of the DSLF annual mean (computed for the 2005–2021 period) obtained with MARS (Figure 4f) shows a very consistent behavior in comparison to the other product datasets. As expected, maximum DSLF values (around 400 Wm^{-2}) are attained over the tropical regions, while minimum values (around 200 Wm^{-2}) are found at higher latitudes. Moreover, overall area means ($\overline{X}$), weighted using the cosine of the latitude, show similar values among all products, where the highest value is obtained with CERES (355 Wm^{-2}); the lowest value with ERA5 (349 Wm^{-2}); while the MARS and MDSLF are very close (354 and 355 Wm^{-2}, respectively). Despite these similarities, systematic differences also occur, including higher values of MDSLF when compared to other estimates (Figures 4b–4d), particularly in South America. These are more significant when compared against ERA5 and CERES (see African, Caspian Sea, and Europe regions); MDSLF clearly tends to generate lower values than the other products at lower ranges of DSLF, between 150 and 200 Wm^{-2} (Figures 4e, 3i and 3m); MARS generally shows higher values than ERA5, with highest values being reached over the Andes mountain range and the Caspian Sea region (Figure 4g), while lower values generated with the DSLF are found over most of the African region and over Brazil when compared with CERES (Figure 4h); generally, CERES presents a higher values in the tropical regions than the remaining products, particularly when compared to ERA5 (Figure 4l), exceeding the highest mean values obtained with MDSLF over the northern Africa and Arabian regions.

The consistency of DSLF estimates using the MARS algorithm as compared with other datasets can also be observed throughout the year and different seasons (see Supporting Information S1). A few differences are worth noting, including the lower MDSLF values during the NH winter period with respect to MARS and ERA5, especially at higher latitudes over the north-eastern Europe region (Figures S1b and S1c in Supporting Information S1, respectively), and also with respect to CERES over north-central Africa (Figure S1d in Supporting Information S1); there are significant higher DSLF values being generated by MDSLF and MARS in comparison to ERA5 over the Caspian Sea region during the NH spring (Figures S2c–S2g in Supporting Information S1), while CERES shows a high increase in the DSLF estimates over North Africa, leading to overall higher values obtained with this product with respect to all others (Figures S2d, S2h, and S2l in Supporting Information S1). The increase of DSLF during the NH summer is clearly pronounced in the MDSLF product, where higher values are generally found over Europe (Figures S3b–S3d in Supporting Information S1), while CERES DSLF is particularly higher than all other estimates over Africa and the Arabian Peninsula. During the NH autumn, the MDSLF product shows higher values with respect to MARS over South America and Central Africa, while slightly lower values are generally found at very high latitudes (Figure S3b in Supporting Information S1).

Figure 5 shows the mean annual cycle of monthly DSLF averaged for the full 2004–2022 period and over land points for group of selected domains (Figure S5 in Supporting Information S1) within the MSG disc, including Europe, North and South Africa, and South America. The results show very similar variations among all datasets

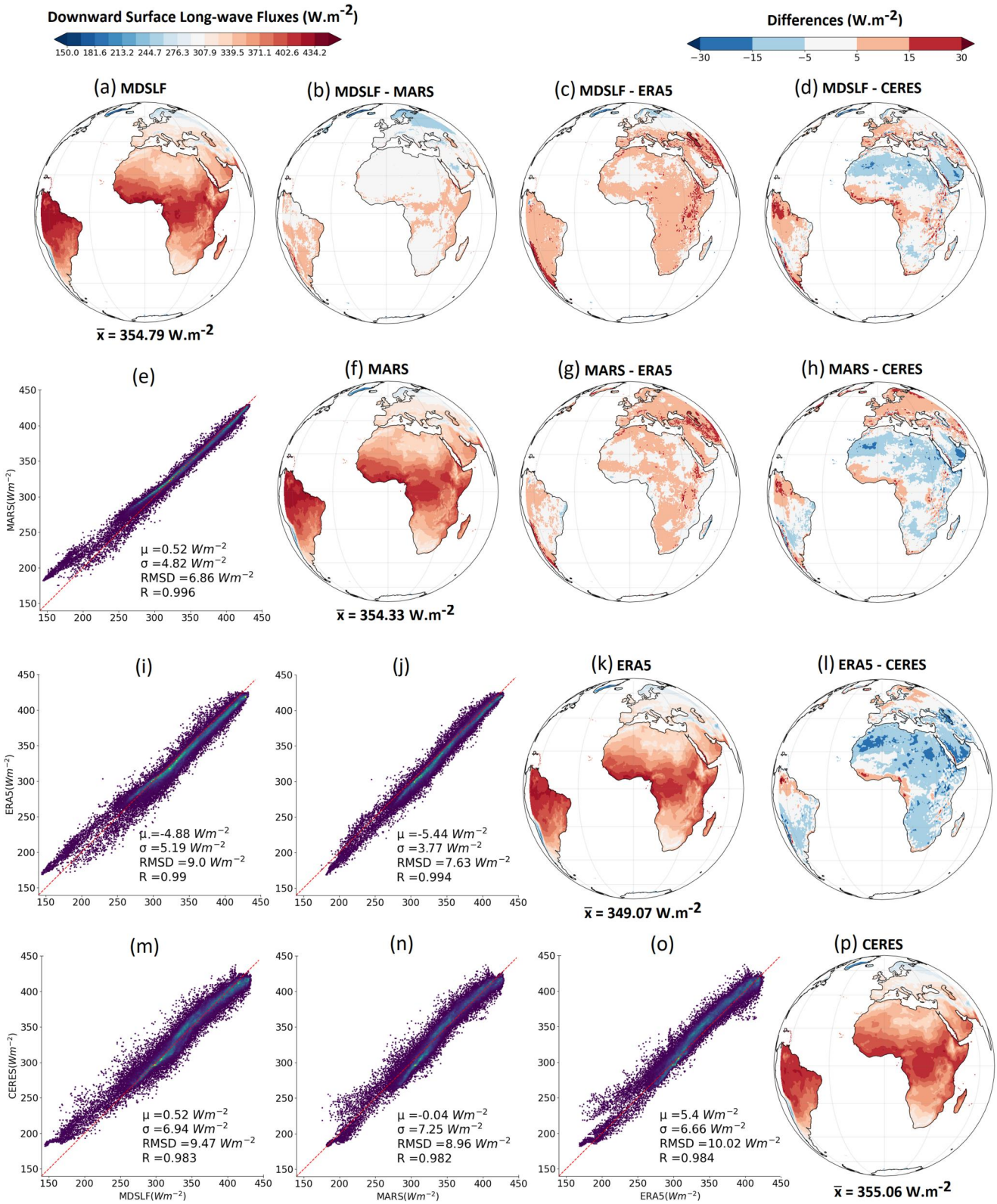

Figure 4. DSLF annual mean estimates for the MSG disc (between 2005 and 2021) produced using different products. Presented outputs include: DSLF spatial distribution maps from MDSLF, MARS, ERA5, and CERES ((a), (f), (k), and (p), respectively), with the overall area weighted mean values ($\overline{x}$); DSLF annual differences maps between products ((b–d), g), (h), and (l); and corresponding density plots ((e), (i), (j), and (m–o)), with error metrics displayed on the inside legend.

21698996, 2024, 6, Downloaded from https://agupubs.onlinelibrary.wiley.com/doi/10.1029/2023JD040306 by ETH Zurich, Wiley Online Library on [08/04/2024]. See the Terms and Conditions (https://onlinelibrary.wiley.com/terms-and-conditions) on Wiley Online Library for rules of use; OA articles are governed by the applicable Creative Commons License

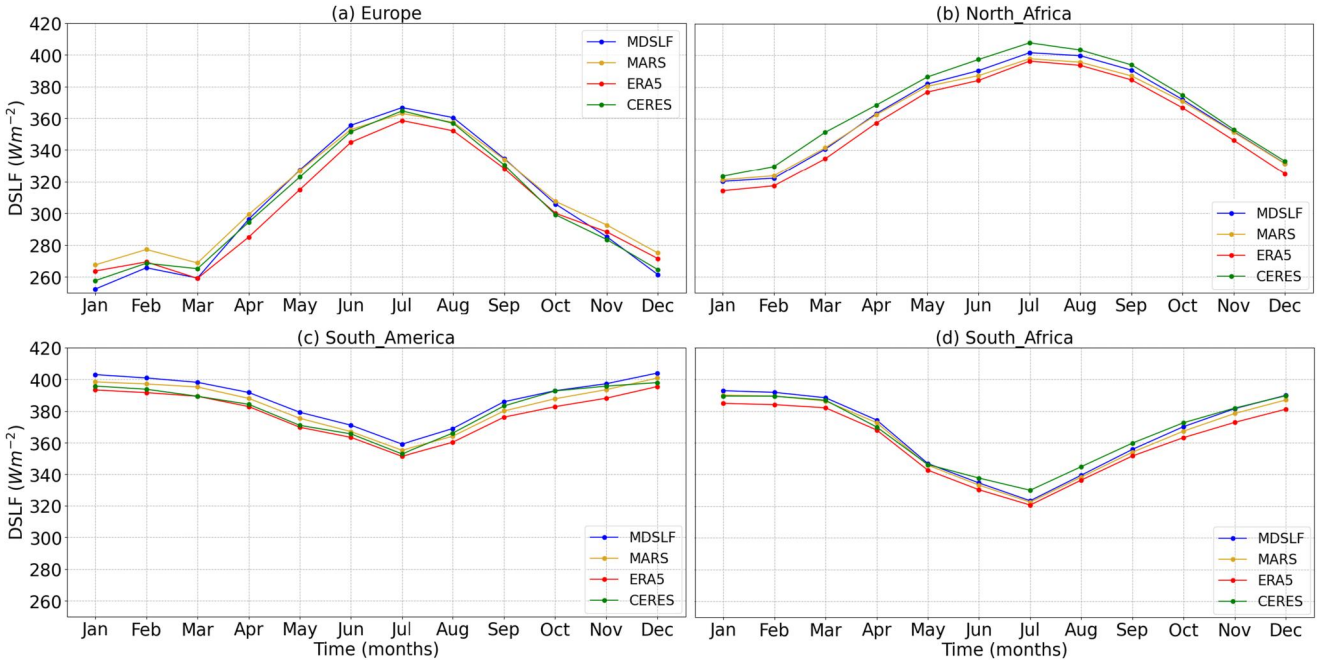

Figure 5. Mean annual cycle (2004–2022) of monthly DSLF (Wm^{-2}) in 4 different regions: (a) Europe; (b) North Africa; (c) South America; and (d) South Africa. DSLF products are depicted by different colors: MDSLF (blue); MARS (yellow); ERA5 (red); and CERES (green). Regions as defined in Figure S5 in Supporting Information S1.

with respect to the mean annual cycle between 2004 and 2022 (Figure 5), with DSLF highest (lowest) values being reached in July for the NH (southern hemisphere, SH) regions. In Europe (Figure 5a) the MARS and MDSLF estimates are very close, particularly throughout the spring and summer periods, when DSLF increases and reaches its highest value in July (around 360 Wm^{-2}). A similar behavior is observed in North Africa (Figure 5b), which generally includes higher DSLF values in comparison, where both MARS and MDSLF also show close behaviors throughout the entire period. CERES mean values are generally characterized by higher DSLF values in comparison to the remaining datasets for North Africa, while the opposed effect is observed in both South America and South Africa regions (Figures 5c and 5d, respectively), with the lowest DSLF values being reached in July (around 360 and 320 Wm^{-2}, respectively). ERA5 generally shows lower DSLF values in the four selected regions when compared to other products. In Figure 6, DSLF annual means over the four selected regions between 2005 and 2021 show very similar inter-annual variability among the different datasets. As shown in Table S2 (see Supporting Information S1), correlation coefficients (R) between MARS and MDSLF annual means with ERA5 are generally found to be significantly higher than with CERES (particularly with the former), which could be partially attributed to the use of ERA5 input variables when computing DSLF. In Europe (Figure 6a), MARS annual mean values follow more closely ERA5 the behavior ($R = 0.96$) than with MDSLF ($R = 0.71$). Other aspects can be highlighted in this region, such as the overall higher DSLF values with the MARS algorithm, and the fact that all datasets except MDSLF seem to reach the highest values of the analyzed period in 2016. As previously noted in the mean annual cycle over North Africa, CERES and ERA5 (Figure 6b) generally show higher and lower DSLF values, respectively, while MARS and MDSLF have a closer behavior through the entire period ($R = 0.92$). Additionally, in this region, a significant (linear) increase of DSLF starts to occur in 2008 for all products, with the maximum value being reached in 2010. In South America (Figure 6c) MARS and MDSLF show a higher degree of consistency between both estimates ($R = 0.97$), particularly until 2015, which is then decreased due to a tendency of the MDSLF algorithm to estimate higher DSLF values in the following years (as opposed to MARS). The MDSLF change from 2015 onwards could be partially attributed to the change of inputs in the algorithm which was previously using ERA-Interim until 2015 and then started to use ECMWF operational forecasts afterward. In South Africa (Figure 6d), a similar behavior occurs to the one found between the different products in the northern region, with an overall increase of correlation between all DSLF products, from which MARS and MDSLF-based annual means show a high correlation ($R = 0.97$).

21698996, 2024, 6, Downloaded from https://agupubs.onlinelibrary.wiley.com/doi/10.1029/2023JD040306 by ETH Zurich, Wiley Online Library on [08/04/2024]. See the Terms and Conditions (https://onlinelibrary.wiley.com/terms-and-conditions) on Wiley Online Library for rules of use; OA articles are governed by the applicable Creative Commons License

Figure 6. Annual means of DSLF (Wm^{-2}) in 4 different regions: (a) Europe; (b) North Africa; (c) South America; and (d) South Africa. DSLF products are depicted by different colored lines: MDSLF (blue); MARS (yellow); ERA5 (red); and CERES (green). Correlation coefficients between the different time series are shown in Table S2 (see in Supporting Information S1).

Finally, a case study to inter-compare the instantaneous spatial patterns of DSLF is shown in Figure 7, with an example of the different DSLF products over the Mediterranean region on 15 July 2021 at 07 UTC with the occurrence of different types of cloud cover. Generally, DSLF patterns follow cloud coverage very closely (both SEVIRI/MSG and ERA5 cloud classification is represented by the light and dark blue pixels in Figures 7e and 7f, respectively), especially the MDSLF and MARS estimates, which are fed with the same satellite information, enabling to follow the granularity of cloudy/partially cloudy patterns. The main differences between ERA5 and SEVIRI-based products (MARS and MDSLF) can be primarily attributed to the differences between satellite cloud identification (Figure 7e) and ERA5 total cloud cover (Figure 7f). In the latter, it is possible to observe a higher occurrence of clouds (e.g., over the Iberian region) in comparison to the satellite information, resulting in lower DSLF values estimated with ERA5 (Figure 7c). The effect of clear/cloudy conditions on the DSLF estimates derived using MARS with inputs from ERA5 and considering MSG cloud classification, has been previously analyzed (Lopes et al., 2022), where MARS values generally have lower errors than ERA5 own downward longwave fluxes. The latter are affected by the misrepresentation of clouds, resulting in higher deviations in comparison to satellite-based products. Figure 7d) is similar to the other products in terms of the general patterns over the region but misses most of the spatial detail due to the coarser grid resolution (1°). It is possible to notice small differences between the MARS and MDSLF fields, where the latter shows a tendency to produce higher DSLF values over large areas (e.g., Northern Africa region and near Greece), as shown in Figure 7b. Figure 7 also highlights the different spatial resolution among products, resulting in smoother spatial characterization of the DSLF (Figure 7c) in comparison to the higher resolution products. This example shows that using high spatial resolution (and temporal frequency) satellite information translates into a significantly higher spatial (and temporal) variability, especially in comparison to fluxes represented by reanalyzes and climate models.

4. Discussion

The validation of the MARS algorithm, now configured to produce instantaneous (30-min) values of DSLF over the whole MSG disc, is shown to be consistent with previous results (Lopes et al., 2022, 2023). Generally, the MARS estimates present better performances than other DSLF products, including the LSA SAF operational

21698996, 2024, 6, Downloaded from https://agupubs.onlinelibrary.wiley.com/doi/10.1029/2023JD040306 by ETH Zurich, Wiley Online Library on [08/04/2024]. See the Terms and Conditions (https://onlinelibrary.wiley.com/terms-and-conditions) on Wiley Online Library for rules of use; OA articles are governed by the applicable Creative Commons License

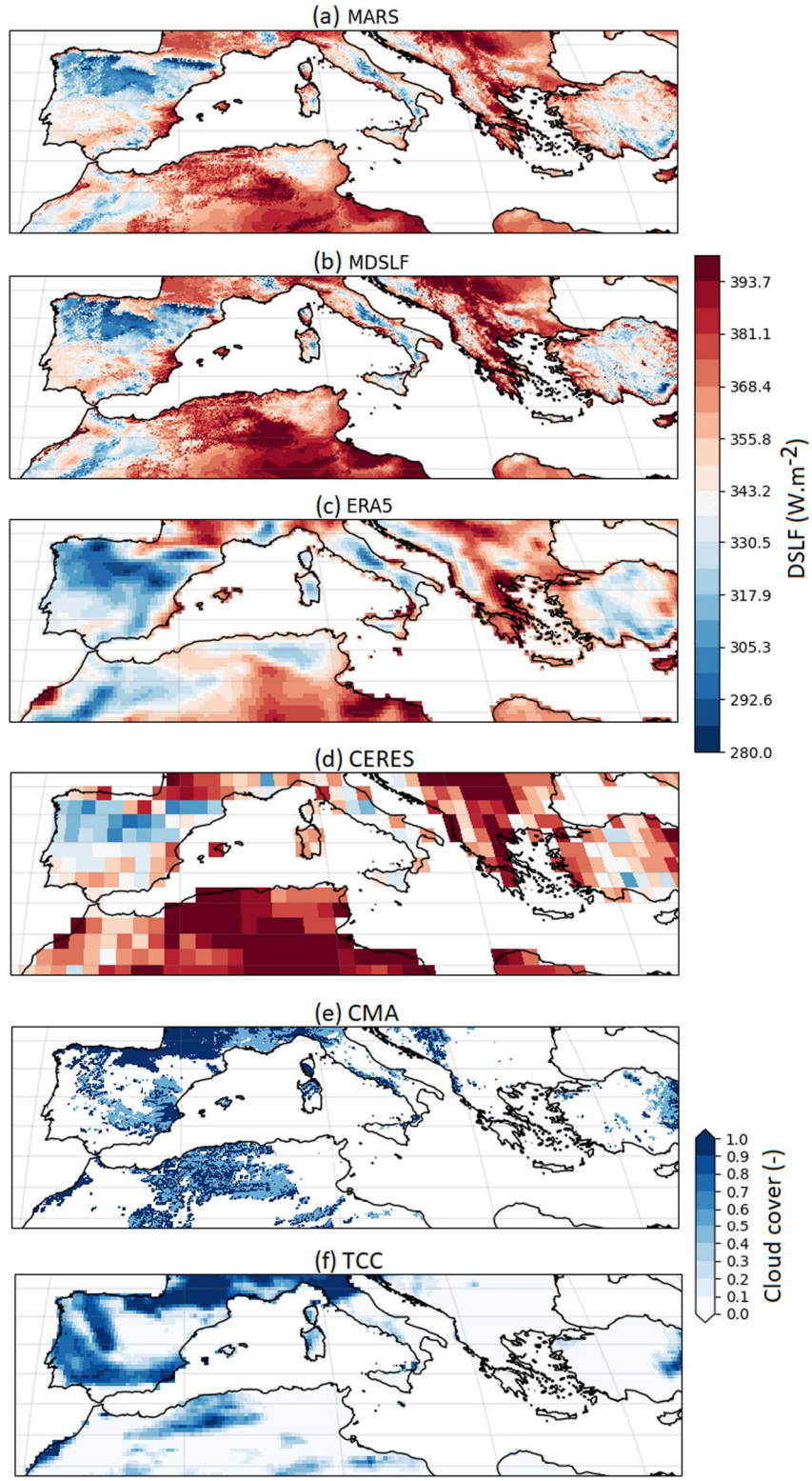

Figure 7. Snapshot of the DSLF hourly distribution over the Mediterranean region on July 15th (2021) at 07 UTC computed with: (a) MARS; (b) MDSLF; and (c) ERA5; and with CERES at 07:30 UTC. Cloud cover information is provided using the MSG cloud mask (CMA) at 15-min instantaneous values (d) and (e) ERA5 hourly total cloud cover (TCC), where cloudy (partially cloudy) sky is depicted by dark (light) blue pixels.

21698996, 2024, 6, Downloaded from https://agupubs.onlinelibrary.wiley.com/doi/10.1029/2023JD040306 by ETH Zurich, Wiley Online Library on [08/04/2024]. See the Terms and Conditions (https://onlinelibrary.wiley.com/terms-and-conditions) on Wiley Online Library for rules of use; OA articles are governed by the applicable Creative Commons License

21698996, 2024, 6, Downloaded from https://agupubs.onlinelibrary.wiley.com/doi/10.1029/2023JD040306 by ETH Zurich, Wiley Online Library on [06/04/2024]. See the Terms and Conditions (https://onlinelibrary.wiley.com/terms-and-conditions) on Wiley Online Library for rules of use; OA articles are governed by the applicable Creative Commons License

product (MDSLF), as shown in Figures 2 and 3. There are several factors that can explain the positive impact of the MARS algorithm, such as: (a) the fact that the algorithm has been calibrated with in situ observations, instead of synthetic longwave flux simulations from MODTRAN-4, as in the case of the current MDSLF product; (b) the flexibility of the MARS algorithm in capturing non-linear relations between near-surface temperature and bulk water vapor content on the one hand, and surface downwelling longwave fluxes on the other, in comparison to simpler methods (such as the piecewise regression used by the MDSLF); and (c) the reliable information on cloud coverage provided in particular by the MSG satellite, which seems to be a critical factor for accurate estimates of DSLF. The evaluation with in situ observations suggest that an empirical algorithm, such as MARS, can produce unbiased estimates of longwave fluxes at the surface using a very limited number of input variables representing surface conditions: air temperature and dew point depression, total column water vapor and accurate cloud coverage information. This relatively simple algorithm is able to produce high-quality DSLF estimates, comparable (or even better) to ERA5, which incorporates a full description of atmospheric profiles and a complex radiation scheme (Morcrette et al., 2008). Moreover, the metrics computed for MARS outperform the CERES product, possibly benefiting from the higher spatial and temporal resolution. Indeed, the validation results presented in Table 2 show the added-value in using the MARS algorithm 0.05° nearest points (MARS*) instead of performing an interpolation to 0.25°, which introduces a slight degradation. These results are in good agreement with other research works (e.g., Feng et al., 2021; Shao et al., 2023) where DSLF estimates produced by a different range of machine learning-based algorithms were generally found to have lower errors than ERA5 and CERES. It is worth noting that between BSRN and FLUXNET2015 monthly validations (Figures 2 and 3, respectively), there is a smaller range of DSLF (i.e., between 250 and 400 Wm^{-2}) being analyzed in the latter. This restriction is due to the fact that all of the 28 FLUXNET2015 stations used are located in Europe, while the station distribution of the 17 BSRN stations covers a wider area. Moreover, larger errors are generally found with FLUXNET2015 for all datasets. This may either be related to the quality of the in situ observations, possibly not following the high standards of BSRN radiation measurements (Mcarthur, 2005), and/or (to a lesser degree) linked to the spatial distribution and range of DSLF values measured in those stations. Nevertheless, it is worth noticing that the MARS performance metrics are very similar for both BSRN stations (where a subset of observations was used for algorithm calibration) and for the completely independent FLUXNET dataset.

The spatial distribution of MARS DSLF annual mean estimates over land points for the whole MSG disc (Figure 4) provides an overview of spatial patterns and their comparison with other datasets for a wide range of climate conditions. This intercomparison exercise does not assume one of the datasets to be an absolute reference, instead allows the investigation of consistencies, as well as the most striking differences among them. All datasets show similar patterns, with maximum DSLF values occurring over low latitudes, particularly at the tropical region of Africa, while minimum values occur over high latitudes, as expected. The MDSLF average values are also similar to those derived from the MARS algorithm, which uses the same input variables as the former. CERES fluxes are generally higher than those of other datasets; such difference seems more pronounced with respect to ERA5 (Figure 4l). Despite the differences in spatial resolution, ERA5 and MARS show a very good agreement without large biases, or conditional biases. In contrast, the currently operational LSA SAF product systematically shows lower DSLF values (generally between 100 and 200 Wm^{-2}), which can be attributed to deficiencies in the training dataset within that range (see density plots (e), (i), and (m), in Figure 4, Figures S1–S4 in Supporting Information S1). This effect is particularly observable during the NH winter (Figures S1b–S1d in Supporting Information S1), when larger areas of DSLF with low values are present within the MSG disc, which conversely nearly disappears during the summer months (Figures S3b–S3d in Supporting Information S1).

The interannual variability of the different datasets (Figure 6) shows consistency among the time series of the MARS, MDSLF, ERA5 and CERES products, that is, high correlations, despite differences in the overall values, being in line with the maps shown in Figure 4. While it can be argued that MARS uses the same ERA5 variables as inputs (i.e., air and dew point temperatures and water vapor), it is known that the actual spatial and temporal variability is driven by cloud cover. The consistency among the three datasets somehow confirms that ERA5 represents well the overall cloud coverage variability. This is further substantiated by the consistency with the CERES fluxes, also heavily relying on satellite data, but yet independent from the remaining products. Nevertheless, the time series shown in Figure 6 reveal systematic differences among the datasets, which themselves vary with the regional domain (being in line with results from Figure 4). These differences may be related to: (a) resolution and the representation of orography in the different datasets (smoothing high mountains may lead to lower values); (b) conditional biases, such as those already identified in MDSLF outputs; (c) limitations arising

21698996, 2024, 6, Downloaded from https://agupubs.onlinelibrary.wiley.com/doi/10.1029/2023JD040306 by ETH Zurich, Wiley Online Library on [08/04/2024]. See the Terms and Conditions (https://onlinelibrary.wiley.com/terms-and-conditions) on Wiley Online Library for rules of use; OA articles are governed by the applicable Creative Commons License

from the MARS/MDSLF empirical approximations, calibration, and input data used; and (d) cloud representation in ERA5 and satellite cloud detection. To further understand the differences among the datasets, a more detailed comparison of temperature, water vapor, and clouds would be necessary, which is currently beyond the scope of this study. However, we note that the maximum differences are on the order of 2%–3%, being well within the commonly acceptable errors for this variable, which has a target accuracy of 5% (10 Wm^{-2}) following BSRN standards (Mcarthur, 2005).

The added-value in using a higher spatial resolution algorithm in comparison to the reanalysis is depicted in Figure 7. As shown for the Mediterranean region, both MARS and MDSLF hourly estimates provide a more detailed characterization of the DSLF spatial variability than ERA5 or CERES, following closely the cloud development over the region; the same characterization can also be applied to the temporal variability representation, following the often-rapid evolution of cloud formation and dissipation, or cloud movement. When compared directly, the MARS and MDSLF products show very similar behaviors with small differences, which are more noticeable in areas where higher DSLF values are to be estimated. Since both algorithms rely on the same inputs to compute DSLF values over the whole MSG disc, the reason for such deviation is mainly related to the differences in algorithms together with the respective adopted calibration procedures. Since cloud cover dominates the high-frequency temporal and spatial variability of DSLF, the use of cloud information from the MSG is considered to be an added value. However, this cannot be fully evaluated since there are no independent high-resolution (temporal and spatial) gridded observations of DSLF.

5. Concluding Remarks

This study focused on the evaluation and intercomparison of four DSLF products: (a) a recently developed all-weather DSLF product based on the multivariate adaptive regression splines (MARS) algorithm driven by satellite cloud information from the Meteosat Second Generation (MSG) and ERA5 reanalysis screen variables; (b) the Satellite Application Facility on Land Surface Analysis (LSA SAF); (c) CERES Synoptic top-of-atmosphere and surface fluxes and clouds (CERES-SYN1deg); and (d) ERA5 reanalysis. The MARS algorithm is aimed to be used in the next version of the LSA SAF operational product to be derived from MSG satellite observations, and in the future by the Meteosat Third Generation (MTG). When in operation, the new LSA SAF DSLF product based on MARS will allow the generation of 30-min instantaneous DSLF values under all-sky conditions and for the whole MSG disc, as tested against other products in this study for the period 2005–2021. Taking advantage of its recursive partitioning and spline fitting, the MARS approach is able to simulate accurate relations between downwelling surface longwave fluxes and screen and bulk atmospheric variables under clear and cloudy conditions, respectively. While near surface air and dew point temperatures and total column water vapor are obtained from ECMWF-ERA5, satellite (MSG) observations provide crucial cloud information for the accurate estimation of DSLF. Moreover, the improvement of the MARS algorithm when compared to the current LSA SAF operational product (MDSLF) can be at least partially attributed to the revision of the calibration dataset, now constituted by in situ observations instead of MODTRAN-4 flux simulations with ERA-40 profiles. Lower errors and higher correlations were found in MARS DSLF estimates through two separate monthly validation analyses using as reference BSRN and FLUXNET2015 datasets, which allowed to reinforce the performance and consistency of the algorithm in comparison to other DSLF products, particularly the current LSA SAF operational product. The fours products were intercompared in terms of their mean spatial variability and temporal mean annual cycles and inter-annual variability in four selected regions, showing a high level of agreement, particularly between MARS, ERA5 and CERES. Our results highlight the clear added value of MARS in respect to LSA SAF, while providing higher spatial resolution (0.05°), constrained by satellite cloud information, when compared with ERA5 (0.25°) or CERES (1°), with the limitation of being restricted to the MSG domain. Overall, these results support the use of the MARS algorithm to generate the new version of the LSA SAF DSLF product, being a reliable alternative to the current operational algorithm, including its future implementation for operations of the MTG satellite.

Data Availability Statement

Observational datasets from the BSRN (Driemel et al., 2018) and FLUXNET2015 (Pastorello et al., 2020) were acquired from the corresponding data centers (https://bsrn.awi.de and https://fluxnet.org, respectively, accessed on 22 January 2024) to elaborate this manuscript. Several DSLF products were used for comparison against the

21698996, 2024, 6, Downloaded from https://agupubs.onlinelibrary.wiley.com/doi/10.1029/2023JD040306 by ETH Zurich, Wiley Online Library on [08/04/2024]. See the Terms and Conditions (https://onlinelibrary.wiley.com/terms-and-conditions) on Wiley Online Library for rules of use; OA articles are governed by the applicable Creative Commons License

MARS estimates, including: the LSA SAF operational product MDSLF (LSA-204; Trigo et al., 2011), acquired from the LSA SAF data server at https://datalsasaf.lsasvcs.ipma.pt/PRODUCTS/MSG/MDSLF/NETCDF/ (accessed on 22 January 2024); ERA5 hourly data (Hersbach et al., 2018), which is available as part of the "ERA5 hourly data on single levels from 1940 to present" was extracted from https://cds.climate.copernicus.eu (accessed on 22 January 2024); and CERES data (Rutan et al., 2015), was obtained from https://ceres.larc.nasa.gov/data (accessed on 22 January 2024). The MARS dataset generated in support of this work is available online in the LSA SAF data server at https://datalsasaf.lsasvcs.ipma.pt/PRODUCTS/MSG/MDSLF_MARS/NETCDF/ (accessed on 22 January 2024), while, in a separate repository, the processed data corresponding to the MARS nearest monthly estimates to observational values and the monthly estimates for the whole MSG domain are made available at Zenodo (Lopes, 2024).

Acknowledgments
We are thankful to the BSRN and the FLUXNET communities for providing the in situ data needed for this study, as well as to Copernicus and ECMWF for making available the forecasted data used. We would also like to thank the availability of CERES-EBAF data obtained from the Atmospheric Science Data Center at the NASA Langley Research Center. F.M.L. acknowledges the funding of the European Union Horizon 2020 research and innovation program under grant agreement No 958927 (CoCO2). This work was performed within the framework of the LSA SAF (http://lsa-saf-eumetsat.int) project, funded by EUMETSAT.

References

Araújo Palharini, R. S., & Vila, D. A. (2017). Climatological behavior of precipitating clouds in the Northeast Region of Brazil. *Advances in Meteorology*, *2017*, 1–12. https://doi.org/10.1155/2017/5916150

Berk, A., Anderson, G. P., Acharya, P. K., Chetwynd, J. H., Bernstein, L. S., Shettle, E. P., et al. (2003). MODTRAN4 Version 3 revision 1 user's manual. In *Air Force Res. Lab; Space Vehicles Directorate, Air Force Material Command: Hanscom Air Force Base, MA, USA*.

Cao, Y., Li, M., & Zhang, Y. (2022). Estimating the clear-sky longwave downward radiation in the Arctic from FengYun-3D MERSI-2 data. *Remote Sensing*, *14*(3), 1–13. https://doi.org/10.3390/rs14030606

Cheng, J., Liang, S., Wang, W., & Guo, Y. (2017). An efficient hybrid method for estimating clear-sky surface downward longwave radiation from MODIS data. *Journal of Geophysical Research*, *122*(5), 2616–2630. https://doi.org/10.1002/2016JD026250

Chevallier, F., Chédin, A., Cheruy, F., & Morcrette, J. J. (2000). TIGR-like atmospheric-profile databases for accurate radiative-flux computation. *Quarterly Journal of the Royal Meteorological Society*, *126*(563), 777–785. https://doi.org/10.1002/qj.49712656319

Diak, G. R., Bland, W. L., Mecikalski, J. R., & Anderson, M. C. (2000). Satellite-based estimates of longwave radiation for agricultural applications. *Agricultural and Forest Meteorology*, *103*(4), 349–355. https://doi.org/10.1016/S0168-1923(00)00141-6

Doelling, D. R., Sun, M., Nguyen, L. T., Nordeen, M. L., Haney, C. O., Keyes, D. F., & Mlynczak, P. E. (2016). Advances in geostationary-derived longwave fluxes for the CERES synoptic (SYN1deg) product. *Journal of Atmospheric and Oceanic Technology*, *33*(3), 503–521. https://doi.org/10.1175/JTECH-D-15-0147.1

Driemel, A., Augustine, J., Behrens, K., Colle, S., Cox, C., Cuevas-Agulló, E., et al. (2018). Baseline Surface Radiation Network (BSRN): Structure and data description (1992-2017) [Dataset]. *Earth System Science Data*, *10*(3), 1491–1501. https://doi.org/10.5194/essd-10-1491-2018

Ellingson, R. G. (1995). Surface longwave fluxes from satellite observations: A critical review. *Remote Sensing of Environment*, *51*(1), 89–97. https://doi.org/10.1016/0034-4257(94)00067-W

Feng, C., Zhang, X., Wei, Y., Zhang, W., Hou, N., Xu, J., et al. (2020). Estimating surface downward longwave radiation using machine learning methods. *Atmosphere*, *11*(1147), 1–20. https://doi.org/10.3390/atmos11111147

Feng, C., Zhang, X., Wei, Y., Zhang, W., Hou, N., Xu, J., et al. (2021). Estimation of long-term surface downward longwave radiation over the global land from 2000 to 2018. *Remote Sensing*, *13*(9), 1848. https://doi.org/10.3390/rs13091848

Feng, H., Wang, S., Xiong, J., Zou, B., & Wang, W. (2023). Variation in the surface radiation budget over different land covers in a subtropical humid region: Evidence from ground observations. *Frontiers in Ecology and Evolution*, *11*(April). https://doi.org/10.3389/fevo.2023.1153733

Feng, H., Ye, S., & Zou, B. (2020). Contribution of vegetation change to the surface radiation budget: A satellite perspective. *Global and Planetary Change*, *192*(February), 103225. https://doi.org/10.1016/j.gloplacha.2020.103225

Friedman, J. H. (1991). Multivariate adaptive regression splines. *Annals of Statistics*, *19*(1), 1–67. https://doi.org/10.1214/aos/1176347963

Friedman, J. H., & Roosen, C. B. (1995). An introduction to multivariate adaptive regression splines. *Statistical Methods in Medical Research*, *4*(3), 197–217. https://doi.org/10.1177/096228029500400303

Hersbach, H., Rosnay, P., Bell, B., Schepers, D., & Al, E. (2018). Operational global reanalysis: Progress, future directions and synergies with NWP [Dataset]. *ERA Report Series*, *27*, 1–63. Retrieved from https://www.ecmwf.int/en/elibrary/80922-operational-global-reanalysis-progress-future-directions-and-synergies-nwp

Hoch, S. W., Whiteman, C. D., & Mayer, B. (2011). A systematic study of longwave radiative heating and cooling within valleys and basins using a three-dimensional radiative transfer model. *Journal of Applied Meteorology and Climatology*, *50*(12), 2473–2489. https://doi.org/10.1175/JAMC-D-11-083.1

Houghton, J. T., Ding, Y., Griggs, D. J., Noguer, M., van Der, L. P. J., Dai, X., et al. (2001). *Contribution of working group I to the third assessment report of the intergovernmental panel on climate change* (p. 94). Cambridge University Press.

Iziomon, M. G., Mayer, H., & Matzarakis, A. (2003). Downward atmospheric longwave irradiance under clear and cloudy skies: Measurement and parameterization. *Journal of Atmospheric and Solar-Terrestrial Physics*, *65*(10), 1107–1116. https://doi.org/10.1016/j.jastp.2003.07.007

Jiang, Y., Tang, B. H., & Zhao, Y. (2022). Estimation of downwelling surface longwave radiation with the combination of parameterization and artificial neural network from remotely sensed data for cloudy sky conditions. *Remote Sensing*, *14*(11), 2716. https://doi.org/10.3390/rs14112716

Jiao, Z. (2022). Estimating all-weather surface longwave radiation from satellite passive microwave data. *Remote Sensing*, *14*(23), 5960. https://doi.org/10.3390/rs14235960

Jung, M., Koirala, S., Weber, U., Ichii, K., Gans, F., Camps-Valls, G., et al. (2019). The FLUXCOM ensemble of global land-atmosphere energy fluxes. *Scientific Data*, *6*(1), 1–14. https://doi.org/10.1038/s41597-019-0076-8

Liou, K.-N. (2002). *An introduction to atmospheric radiation* (2nd ed.). Academic Press. https://doi.org/10.1016/s0074-6142(13)62909-5

Lopes, F. (2024). MARS DSLF estimates over the MSG domain between 2004 and 2022 [Dataset]. *Zenodo*. https://doi.org/10.5281/zenodo.10462598

Lopes, F. M., Dutra, E., & Trigo, I. (2022). Integrating reanalysis and satellite cloud information to estimate surface downward long-wave radiation. *Remote Sensing*, *14*(1704), 1704. https://doi.org/10.3390/rs14071704

Lopes, F. M., Dutra, E., & Trigo, I. (2023). *Machine learn estimates of downward surface long-wave fluxes (Dslf) based on reanalysis and satellite observations*. In L. B. Mário Gonzalez Pereira, R. Oliveira, & P. Navarro (Eds.), *Advances in meteorology and geophysics* (pp. 22–28). APMG2023. https://doi.org/10.60620/he5s-8x66

Marty, C., Philipona, R., Frøhlich, C., & Ohmura, A. (2002). Altitude dependence of surface radiation fluxes and cloud forcing in the Alps: Results from the alpine surface radiation budget network. *Theoretical and Applied Climatology*, *72*(3–4), 137–155. https://doi.org/10.1007/s007040200019

Mcarthur, L. J. B. (2005). *World Climate Research Programme Baseline Surface Radiation Network (BSRN) operations manual version 2.1*. International Oceanographic Commission of Unesco.

Meloni, D., Di Biagio, C., Di Sarra, A., Monteleone, F., Pace, G., & Sferlazzo, D. M. (2012). Accounting for the solar radiation influence on downward longwave irradiance measurements by pyrgeometers. *Journal of Atmospheric and Oceanic Technology*, *29*(11), 1629–1643. https://doi.org/10.1175/JTECH-D-11-00216.1

Morcrette, J. J., Barker, H. W., Cole, J. N. S., Iacono, M. J., & Pincus, R. (2008). Impact of a new radiation package, McRad, in the ECMWF integrated forecasting system. *Monthly Weather Review*, *136*(12), 4773–4798. https://doi.org/10.1175/2008MWR2363.1

Obot, N. I., Humphrey, I., Chendo, M. A. C., & Udo, S. O. (2019). Deep learning and regression modelling of cloudless downward longwave radiation. *Beni-Suef University Journal of Basic and Applied Sciences*, *8*(1), 23. https://doi.org/10.1186/s43088-019-0018-8

Ojo, O. S., Adeyemi, B., & Ogolo, E. O. (2019). Assessments of the night-time and daytime radiative fluxes balance on seasonal timescale over West Africa. *Journal of Atmospheric and Solar-Terrestrial Physics*, *191*(April 2018), 105048. https://doi.org/10.1016/j.jastp.2019.05.012

Pastorello, G., Trotta, C., Canfora, E., Chu, H., Christianson, D., Cheah, Y. W., et al. (2020). The FLUXNET2015 dataset and the ONEFlux processing pipeline for eddy covariance data [Dataset]. *Scientific Data*, *7*(1), 225. https://doi.org/10.1038/s41597-020-0534-3

Roesch, A., Wild, M., Ohmura, A., Dutton, E. G., Long, C. N., & Zhang, T. (2011). Assessment of BSRN radiation records for the computation of monthly means. (pp. 339–354). https://doi.org/10.5194/amt-4-339-2011

Rutan, D. A., Kato, S., Doelling, D. R., Rose, F. G., Nguyen, L. T., Caldwell, T. E., & Loeb, N. G. (2015). CERES synoptic product: Methodology and validation of surface radiant flux [Dataset]. *Journal of Atmospheric and Oceanic Technology*, *32*(6), 1121–1143. https://doi.org/10.1175/JTECH-D-14-00165.1

Shao, J., Letu, H., Ri, X., Tana, G., Wang, T., & Shang, H. (2023). Estimation of surface downward longwave radiation and cloud base height based on infrared multichannel data of Himawari-8. *Atmosphere*, *14*(3), 493. https://doi.org/10.3390/atmos14030493

Silber, I., Verlinde, J., Wang, S. H., Bromwich, D. H., Fridlind, A. M., Cadeddu, M., et al. (2019). Cloud influence on ERA5 and AMPS surface downwelling longwave radiation biases in West Antarctica. *Journal of Climate*, *32*(22), 7935–7949. https://doi.org/10.1175/JCLI-D-19-0149.1

Trigo, I. F., Barroso, C., Viterbo, P., Freitas, S. C., & Monteiro, I. T. (2010). Estimation of downward long-wave radiation at the surface combining remotely sensed data and NWP data. *Journal of Geophysical Research*, *115*(24), 1–14. https://doi.org/10.1029/2010JD013888

Trigo, I. F., Monteiro, I., & Freitas, S. C. (2011). The EUMETSAT Satellite Application Facility on Land Surface Analysis (LSA SAF). Validation report. In *Down-welling Longwave Flux (MDSLF) (Issue I)*. Retrieved from https://nextcloud.lsasvcs.ipma.pt/s/JXNeANe6bgXE8Px

Wang, K., & Dickinson, R. E. (2013). Global atmospheric downward longwave radiation at the surface from ground-based observations, satellite retrievals, and reanalyses. *Reviews of Geophysics*, *51*(2), 150–185. https://doi.org/10.1002/rog.20009

Wang, T., Shi, J., Ma, Y., Letu, H., & Li, X. (2020). All-sky longwave downward radiation from satellite measurements: General parameterizations based on LST, column water vapor and cloud top temperature. *ISPRS Journal of Photogrammetry and Remote Sensing*, *161*(April 2019), 52–60. https://doi.org/10.1016/j.isprsjprs.2020.01.011

Wang, T., Yan, G., & Chen, L. (2012). Consistent retrieval methods to estimate land surface shortwave and longwave radiative flux components under clear-sky conditions. *Remote Sensing of Environment*, *124*, 61–71. https://doi.org/10.1016/j.rse.2012.04.026

Wild, M., Folini, D., Scha, C., Loeb, N., Dutton, E. G., & Ko, G. (2013). The global energy balance from a surface perspective (pp. 3107–3134). https://doi.org/10.1007/s00382-012-1569-8

Wild, M., Ohmura, A., Gilgen, H., Morcrette, J. J., & Slingo, A. (2001). Evaluation of downward longwave radiation in general circulation models. *Journal of Climate*, *14*(15), 3227–3239. https://doi.org/10.1175/1520-0442(2001)014<3227:EODLRI>2.0.CO;2

Zeng, Q., Cheng, J., Member, S., & Dong, L. (2020). Assessment of the Long-Term High-Spatial-Resolution Global LAnd Surface Satellite (GLASS) surface longwave radiation product using ground measurements. *Ieee Journal of Selected Topics in Applied Earth Observations and Remote Sensing*, *13*, 2032–2055. https://doi.org/10.1109/JSTARS.2020.2992472

Zhang, T., Stackhouse, P. W., Gupta, S. K., Cox, S. J., & Mikovitz, J. C. (2015). The validation of the GEWEX SRB surface longwave flux data products using BSRN measurements. *Journal of Quantitative Spectroscopy and Radiative Transfer*, *150*, 134–147. https://doi.org/10.1016/j.jqsrt.2014.07.013

Zhao, W., Kuhn, W. R., & Drayson, S. R. (1994). The significance of detailed structure in the boundary layer to thermal radiation at the surface in climate models. *Geophysical Research Letters*, *21*(15), 1631–1634. https://doi.org/10.1029/94GL01393

Zhong, L., Zou, M., Ma, Y., Huang, Z., Xu, K., Wang, X., et al. (2019). Estimation of downwelling shortwave and longwave radiation in the Tibetan plateau under all-sky conditions. *Journal of Geophysical Research: Atmospheres*, *124*(21), 11086–11102. https://doi.org/10.1029/2019JD030763

Zhou, W., Shi, J., Wang, T., Peng, B., Zhao, R., & Yu, Y. (2019). Clear-sky longwave downward radiation estimation by integrating MODIS data and ground-based measurements. *Ieee Journal of Selected Topics in Applied Earth Observations and Remote Sensing*, *12*(2), 450–459. https://doi.org/10.1109/JSTARS.2018.2878229

Zhou, W., Wang, T., Shi, J., Peng, B., Zhao, R., & Yu, Y. (2018). Remotely sensed clear-sky surface longwave downward radiation by using multivariate adaptive regression splines method. *IEEE*, 5575–5578.

21698996, 2024, 6, Downloaded from https://agupubs.onlinelibrary.wiley.com/doi/10.1029/2023JD040306 by ETH Zurich, Wiley Online Library on [08/04/2024]. See the Terms and Conditions (https://onlinelibrary.wiley.com/terms-and-conditions) on Wiley Online Library for rules of use; OA articles are governed by the applicable Creative Commons License